CHAPTER 2

Recognition of images of blood cells using texture and neural networks to diagnose leukemia

Airam Curtidor
Masuma Mammadova
Graciela Velasco Herrera
Tetyana Baydyk
Ernst Kussul

Abstract

Analysis of white blood cells from blood can help to detect Acute Lymphoblastic Leukemia, a potentially fatal blood cancer if left untreated. The morphological analysis of blood cells images is typically performed manually by an expert; however, this method has numerous drawbacks, including slow analysis, low precision, and the results depend on the operator's skill.

We have developed and present here an automated method for the identification and classification of white blood cells using microscopic images of peripheral blood smears. Once the image has been obtained, we propose describing it using brightness, contrast, and micro-contour orientation histograms. Each of these descriptions provides a coding of the image, which in turn provides *n* parameters. The extracted characteristics are presented to an encoder's input. The encoder generates a high-dimensional binary output vector, which is presented to the input of the neural classifier.

This paper presents the performance of one classifier, the Random Threshold Classifier. The classifier's output is the recognized class, which is either a healthy cell or an Acute Lymphoblastic Leukemia-affected cell. As shown below, the proposed neural Random Threshold Classifier achieved a recognition rate of 98.3 % when the data has partitioned on 80 % training set and 20 % testing set for.

Our system of image recognition is evaluated using the public dataset of peripheral blood samples from Acute Lymphoblastic Leukemia Image Database. It is important to mention that our system could be implemented as a computational tool for detection of other diseases, where blood cells undergo alterations, such as Covid-19.

 DOI: 10.21303/978-9916-9850-2-1.ch2

Keywords
Image processing, segmentation of microscopic images, cell analysis, detection of white blood cells, leukemia classification, neural classifiers.

2.1 Introduction

Artificial Intelligence (AI) is currently used in a wide variety of fields, including the medical field. With the aid of various AI techniques, specialized software for the early diagnosis of diseases can be developed [1–3].

In this study AI techniques are applied to analyze and recognize images captured by a microscope of human peripheral blood smear samples. A tool will be developed using computer vision and neural networks to help detect possible changes in the size and shape of the different blood cells, with a focus on lymphocytes, for the detection of Acute Lymphoblastic Leukemia (ALL) [4]. This tool could be used for the detection of other diseases, where there are changes in the morphology of blood cells, for example, the analysis of peripheral blood offers valuable information in the hematology diagnostic process. The morphological assay can add information about the pathophysiology of COVID-19 disease and its progression. In this type of analysis, hematological abnormalities that occur in patients affected by severe viral pneumonia with clinical consequences that can end in multiple organ failure were detected [5–8].

A normal blood consists of three main components: red blood cells (erythrocytes), white blood cells (WBC) or leukocytes, and platelets. Leukocytes are easily distinguishable due to the fact that their nuclei are darker than the background. Granulocytes are leukocytes containing granules, including neutrophils, basophils, and eosinophils. Cells without granules are called mononuclear and include lymphocytes and monocytes, **Fig. 2.1, *a***. The percentage of lymphocytes in human blood ranges from 20 % to 45 %, and their size ranges from 7 to 15 micrometers. They are distinguished by a round nucleus and poor cytoplasm. ALL affects a group of leukocytes called lymphocytes and is caused by the excessive production of immature white blood cells called lymphoblasts (also known as blastic cells), which inhibit the production of normal white blood cells. L1, L2, L3 are three classes of lymphoblasts shown in the **Fig. 2.1, *b***. In detail we will describe this lymphoblasts classification and the image database in paragraph 2.4. ALL lymphoblasts are characterized by additional morphological alterations that exacerbate the severity of the disease. In particular, lymphocytes have a regular shape and a compact nucleus with regular and continuous borders. In contrast, lymphoblasts have an irregular shape and contain small cavities

in the cytoplasm, called vacuoles, and spherical particles within the nucleus, called nucleoli [9]. Leucocyte classification for leukemia detection using Image Processing Techniques (IPT) was proposed in [10].

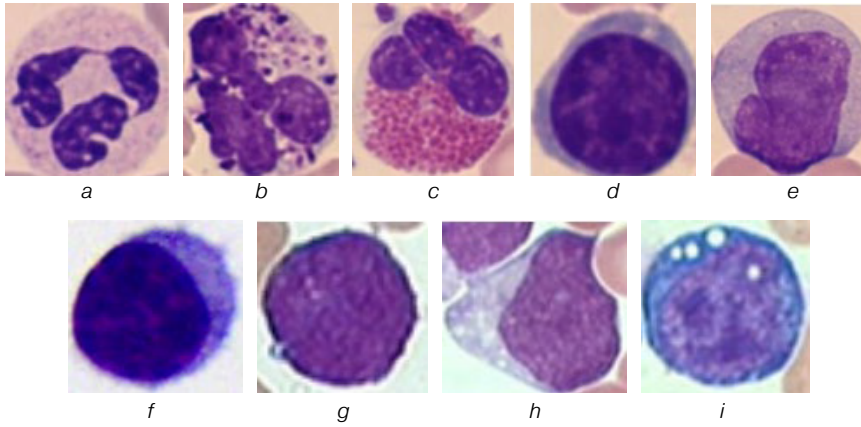

Fig. 2.1 White blood cells (leukocytes): *a–e* comparison between various white blood cell types, including neutrophils, basophils, eosinophils, lymphocytes, and monocytes; *f–i* comparison between lymphocytes with ALL: a healthy lymphocyte followed by lymphoblasts classified as L1, L2, and L3, respectively [4]

Cells in human blood can be counted using image processing techniques, which at the same time may provide information on cell morphology. A system for the automatic detection of ALL-affected cells is first based on image acquisition using a camera attached to a microscope. Then the image is subjected to preprocessing or image enhancement to eliminate noise or any factor that may interfere with the performance of the subsequent stages. And finally, the segmentation process starts, which consists of dividing an image into its constituent regions or objects. The most challenging task in image processing is the segmentation of complex images, such as blood cells, due to their complex nature and overlapping of these cells. Then from each cellular component, different characteristics, such as shape, color, and/or texture as well as their combinations, most of which are problem-specific, are extracted, and the classifier will detect ALL-affected lymphocytes or not from this data.

Various algorithms have been proposed for separating leukocytes and erythrocytes, as well as their classification as normal or abnormal, based on certain morphological characteristics of the cells, including the analysis of the nucleus in the case of leukocytes. The problem of white blood cell identification and classification

is focused in [11]. The proposed system first separates leukocytes from other blood cells in the blood image, then extracts morphological indices, and finally classifies the leukocytes using a neural classifier.

To improve the image, low-pass, and band-pass filters are applied to reduce noise if they do not have good illumination [12]. The authors focus on the segmentation process of blood images to extract significant parts or regions of interest and propose an intuitionistic fuzzy set approach for optimal threshold selection based on histogram calculations. This method is then extended to perform multiple thresholding to account for possible local variations in the image. The proposed method is evaluated on peripheral blood images to subdivide the various image components, where excellent segmentation and speed performance are demonstrated.

Using active contour models that are initialized with morphological operators, cells are segmented in [13]. Functions based on shape and texture are used for classification. Different classifiers are employed, such as K-nearest neighbors, learning vector quantization, multilayer perceptron and support vector machine. This automated differential blood counter system employs statistical and neural network-based classification methods to try to perform Differential Blood Count (DBC) automatically.

An effective technique for automatically segmenting blood cell nuclei is described in [14]. The technique is based on the enhancement and filtering of grayscale contrast. A minimum segment size is implemented to eliminate false objects. The technique is evaluated using 365 blood images. The segmentation performance is evaluated quantitatively as 79.7 % on the test set. Each of the five normal white blood cell types is evaluated individually to compare performance. The lowest segmentation precision is for eosinophils at 69.3 %, and the highest is for monocytes at 86.3 %.

A very detailed review of the different proposals reported in the literature on methods of segmentation, extraction of characteristics, and classification of white blood cells or leukocytes is presented in [15].

There is paper that focuses on white blood cell nucleus segmentation, which separates the nucleus from the cell body by utilizing a combination of automatic contrast stretching supported by arithmetic image operations, minimal filtering, and global thresholding techniques [16].

An image processing technique for automatic blast number counting is proposed in [17]. Using segmentation based on the HSV color space, white blood cells (WBC) are extracted from the background. A simple morphological operator, such as erosion, plays a crucial role, particularly for overlapping cells.

Various segmentation techniques, such as, Hough transform, thresholding techniques, boundary-based segmentation, and region-based segmentation, have been proposed to achieve efficient and accurate results [18–20].

A method for segmenting color images is demonstrated in [21]. Color images provide a more accurate description of a scene than grayscale images because they are a richer source of information.

A system was proposed in which the first separates the leukocytes from the other blood cells was made, then the lymphocytes (cells of interest to detect acute leukemia) were selected, the morphological indices of those cells were evaluated, and the presence of leukemia finally was classified, the morphological indices in three steps: processing first the membrane, then the cytoplasm and finally the nucleus were extracted [22].

An instrument for segmenting and identifying red and white blood cells from an image was provided [23]. This project used color-based segmentation with $L^*a^*b^*$ (CIELAB) color space to perform segmentation. In this work, the accuracy ranges from 64 % to 87 % depending on the type of processing used and the type of cells being extracted.

Tests on public datasets for leukemia detection, SMC-IDB, IUMS-IDB, and ALL-IDB, were conducted and achieved an ALL-classification accuracy of 94.1 % [24]. This research implements image processing techniques to automate the counting and classification of blood cells, specifically white blood cells, as leukemia-affected or not. To better visualize the leukocytes in a blood image, they perform image preprocessing, implement an algorithm that provides useful information about the location of candidate leukocytes, and segment the image into regions of interest using Otsu's algorithm and the watershed algorithm. Then, the characteristics extraction was performed using a convolutional neural network (CNN) that had been pre-trained, followed by binary classification (ALL-affected and unaffected leukocytes) using a linear support vector machine. One of the ways to increase the accuracy and speed of recognition algorithms is to use a convolutional neural network (CNN). It was introduced a CNN in conjunction with a Kohonen network, the first to provide the system with the ability to detect and recognize objects and the second to find areas of interest. The combination of the above methods allows to speed up the process of searching and recognizing objects in images [25, 26].

There are different proposals to detect ALL using different artificial intelligence methodologies. They use the ALL-IDB database [27]. This database is popular to compare different methods and algorithms. We will analyze the results that were obtained with this image database.

There was proposed and developed the algorithms using image segmentation and data mining algorithms and showed the classification of the acute lymphoblastic leukemia into its three respective categories namely: L1, L2, L3, achieved an overall accuracy of 98.6 % [28]. The segmentation process is automatic using K-medoids

algorithm, they extracted the cytoplasm from the images without involving manual cropping procedure. Their approach is based on extracting shape, visual and texture features like area cytoplasm, area nucleus, nucleus-cytoplasm relation, size of the blast, vacuoles, entropy and contrast of the image, among others. For classification and prediction, the Random Forest (RF) algorithm presented the best results [28].

It was used fuzzy c-means (FCM) clustering for nuclei segmentation [29]. They extracted, five geometrical features (area, perimeter, solidity, eccentricity and extent) and, 36 statistical features (mean, standard deviation, energy, entropy, skewness and kurtosis) are calculated from the image histogram of the red, green and blue, plus the hue, saturation and enhanced value channels from the pixels located in nuclei, respectively. In this way they obtained 41 components and selected 13 of the best features. For the classification of L1, L2, L3, normal, reactive and atypical cells, RF classifier was applied and result was in 98 % accuracy. They propose in the future, in addition of nuclei, segmentation of cytoplasm and extraction its features to improve accuracy of their system [29].

It was proposed a hybrid model based on deep convolutional neural networks (CNNs) and a deep residual network named ResNet-50 V2 [30], to predict ALL. They trained the deep residual network using the optimized hyperparameters by genetic algorithms (GA), reaching higher performance against approaches without optimization and optimization using random search and Bayesian algorithms [31]. The results show that the GA optimization improves the accuracy of the classifier, obtaining 98.46 %.

A novel deep learning framework (DLF) based on convolution neural network was proposed [32]. The authors did two experiments: in one of them they obtained 98.62 % when the data has been partitioned on training and testing sets as 80 % and 20 %, and in the second experiment they obtained 97.73 % when the data has been partitioned as training and testing images as 60 % and 40 %.

It was proposed an improved Adaptive Network-Based Fuzzy Inference Systems (ANFIS) model to predict leukemia data using an Euclidean distance to measure between the trained feature data and the test feature data [33]. An Improved Adaptive Neuro-Fuzzy Neural Network (ANFNN) is also introduced, which helps the input space be partitioned into many local regions by the fuzzy clustering, in which the computation complexity is decreased and, based on both the separation and the compactness among the clusters, the fuzzy rule number is determined by the validity function. Improved ANFIS obtained the best accuracy of 97.14 %.

Classification of white blood cells into healthy and unhealthy using Support Vector Machine (SVM) learning model was presented in [34]. Image features are extracted with transfer learning approach of deep convolutional neural network

using AlexNet pretrained model. AlexNet is an eight layered convolutional neural network. This model is introduced by Alex Krizhevsky at University of Toronto in 2010 [35]. This approach validates the process of discriminating white blood cells into healthy and acute lymphoblastic leukemia affected unhealthy cells with 96.15 % of accuracy.

A computer-aided automated diagnosis system for detection of acute lymphoblastic leukemia (ALL) using deep-learning models is discussed in [36]. A pretrained AlexNet model is deployed for performing this task. The work implemented in this paper does not require any preprocessing, the raw image is fed in this model for performing both feature extraction and classification task. This proposed method achieves an accuracy of 98 %.

A micro-pattern descriptor, called Local Directional Number Pattern (LDNP) along with Multi-scale Weber Local Descriptor (MWDT) for feature extraction task to determine cancerous and noncancerous blood cells are discussed and presented in [37].

It was applied different individual and combined feature extraction methods, and fed into the machine learning classifiers (Decision Tree, Ensemble, K-Nearest Neighbors, Naive Bayes, and RF) and presented an average classification accuracy 97.69 % using Ensemble classifier.

We can summarize the introduction with a conclusion regarding the relevance of this issue, based on a review of tasks, approaches and methods for medical image recognition and classification. The task of medical images recognition is actual and important.

2.2 Materials and methods

Currently, there are various approaches and methods to solve the task of medical images recognition which are closer to our approach.

The k-means clustering algorithm for segment the images. Based on the colour, texture and shape the image pixels are grouped as three clusters. The texture features were extracted as Grey Level Co-Occurrence Matrix (GLCM) and Local Binary Pattern (LBP) are used in [38]. Support vector machine (SVM) with Gaussian radial basis function (RBF) as kernel is used for classification. They obtained an accuracy of 95.3 % for ALL-IDB2 database.

So, last years' active attention of scientists and engineers is attracted to the problem of automatic recognition and classification of blood cells for different types of diseases. Analysis of WBC from blood can help to detect ALL, COVID-19 disease or other illness.

We have proposed an automated method for the identification and classification of white blood cells using microscopic images of peripheral blood smears and neural Random Threshold Classifier (RTC).

The first application of the RTC for medical image recognition was realized for Chagas recognition [1, 39]. Chagas disease is caused by the *Trypanosoma cruzi* parasite and affects both humans and domestic animals, and the vector for introduction into the human body is a bedbug. This insect usually lives in gardens, jungles and especially on thatched roofs and dirt floors. In **Fig. 2.2, *a*** we present the sample of infected tissue.

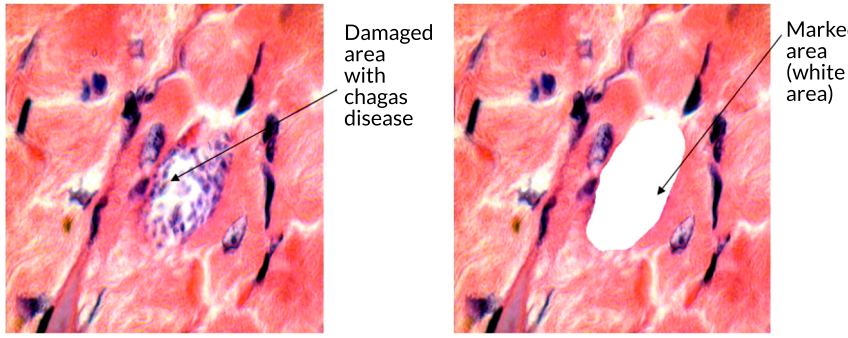

Fig. 2.2 Tissue with Chagas: *a* – infected tissue; *b* – marked image

At our disposal we have a set of 10 images with tissue damaged by Chagas disease in BMP format (Bitmap) with a resolution of 533×400 pixels and a size of 625 KB.

As inputs for our neural RTC classifier we used texture features. Texture features algorithm was developed on the base of calculation of histograms of brightness (analysis of every pixel), contrast (analysis of two adjacent horizontal or vertical pixels and calculation of their brightness differences), and contour orientations (analysis of four, 9 or 16 adjacent pixels). The orientation of contours on the image can be calculated with help of Schwartz (Paragraph 2.2.1), Sobel, or Roberts algorithms [40, 41]. On the base of these results, we can calculate histograms of contour orientations.

The training and validation of the system was carried out using a base of 10 images: 5 of which were used for training and 5 were used for recognition. The best recognition percentage was 97.54 %.

2.2.1 Calculation of the contour orientation on an image

To calculate the orientation of contours in the image, we used the algorithm, based on Schwartz's [40] patent for analogous electronic schematics. We have adapted his proposal for computer calculations.

This algorithm works on square arrays of four adjacent pixels whose brightness is known (**Fig. 2.3**).

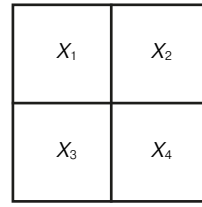

Fig. 2.3 Four pixels for analysis

The algorithm has several steps:

1. We choose four pixels. Each value from $X1$ to $X4$ corresponds to a brightness value, this value can go from 0 to 255 (in case eight bits are used for encoding).

2. Two new variables of $Y1$ and $Y2$ are used; these values correspond to the sum of the brightness values diagonally (**Fig. 2.4**).

Therefore, the following equations are obtained:

$$Y_1 = X_1 + X_4, \tag{2.1}$$

$$Y_2 = X_2 + X_3.$$

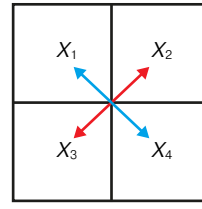

Fig. 2.4 Diagonal elements

3. Additionally, a value for a constant C is chosen (for this task a constant value of 10 is used).

This value is experimental and the one that will work as an indicator of whether or not there is any contour in this place.

If $Y_1 - Y_2 > C$, outline does not exist and we have to analyze the next four pixels (step 1).

If $Y_1 - Y_2 \approx C$, the contour can exist and we have to calculate the angle of its orientation (step 4).

4. Now the difference between the values of the pixels is calculated diagonally, and they are assigned to the variables δ_1 and δ_2:

$$\delta_1 = X_1 - X_4, \tag{2.2}$$

$$\delta_2 = X_2 - X_3.$$

5. Now the minimum value and the maximum value of the absolute values of the variables δ_1 and δ_2 are established and are assigned to variables θ_1 and θ_2, respectively:

$$\theta_1 = \min(|\delta_1|, |\delta_2|), \tag{2.3}$$

$$\theta_2 = \max(|\delta_1|, |\delta_2|).$$

6. From the absolute values of these differences, the maximum and minimum are obtained and we make the quotient:

$$Y = \frac{\theta_1}{\theta_2}. \tag{2.4}$$

Value of Y will always be less than 1.

7. **Table 2.1** indicates eight octants. According to the signs of the parameters δ_1, δ_2, and $|\delta_1| - |\delta_2|$. **Table 2.1** is established, which will indicate the interval in which the contour orientation angle is found.

Table 2.1 Calculations of angle orientations

φ	$\left(0, \frac{\pi}{4}\right)$	$\left(\frac{\pi}{4}, \frac{\pi}{2}\right)$	$\left(\frac{\pi}{2}, \frac{3\pi}{4}\right)$	$\left(\frac{3\pi}{4}, \pi\right)$	$\left(\pi, \frac{5\pi}{4}\right)$	$\left(\frac{5\pi}{4}, \frac{3\pi}{2}\right)$	$\left(\frac{3\pi}{2}, \frac{7\pi}{4}\right)$	$\left(\frac{7\pi}{4}, 2\pi\right)$
				Y				
δ_1	+	+	+	–	–	–	–	+
δ_2	–	+	+	+	+	–	–	–
$\lvert\delta_1\rvert - \lvert\delta_2\rvert$	+	+	–	–	+	+	–	–

Depending on the combination of signs, the value of *Y* will be added or subtracted from the dividing line corresponding to $\pi/4$, $3\pi/4$, $5\pi/4$ or $7\pi/45$, depending on the case indicated in the **Table 2.1**.

Example:

1) adjacent pixels:

4	3
2	1

Therefore:

$X_1 = 4, X_2 = 3$ and $X_3 = 2, X_4 = 1$;

2) it is calculated $Y_1 = X_1 + X_4 = 4+1 = 5$, $Y_2 = X_2 + X_3 = 3+2 = 5$;

3) it is compared with the value of the constant *C* (for this case it is 10). In this case the values of $Y_1 = 5$ and $Y_2 = 5$ show that the contour exists;

4) the values of δ_1 and δ_2:

$\delta_1 = X_1 - X_4 = 4-1 = 3$, $\delta_2 = X_2 - X_3 = 3-2 = 1$;

5) the maximum and minimum of δ_1 and δ_2 are θ_1 and θ_2:

$\theta_1 = 3$; $\theta_2 = 1$;

6) The value of *Y* is calculated:

$Y = 1/3$.

By using **Table 2.1** and based on the conditions obtained, that is, the signs of δ_1, δ_2, and $|\delta_1| - |\delta_2|$, that all three have "+" we are in the second octant. In this case, since all the signs of our variables are positive, we can deduce that the orientation of the contour is between $\pi/4$ and $\pi/2$. The actual value is calculated as $\pi/4 + Y = 0.785 + 0.33 = 1.115$ radians.

2.2.2 Other algorithms of texture recognition

Other algorithms were developed for calculating texture characteristics on the image and tested [42]. It was proposed an algorithm for finding a set of texture features characterizing the most homogeneous texture area of an input image. The found set of features was intended for extraction of this segment. The algorithm, developed by A. Goltsev, processed any input images in the absence of any preliminary information about the images and, accordingly, without any learning.

The essence of the algorithm is as follows. The image is covered with a number of test windows. In each of them, a degree of texture homogeneity is measured. The test window with maximal degree of homogeneity is determined and a representative patch of pixels is detected. The texture features extracted from the detected representative patch is considered as those that best characterize the most homogeneous texture segment. The example of work of the developed algorithm is presented in **Fig. 2.5**.

a *b* *c*

Fig. 2.5 Textures of black cat and tree:
a – original image; *b* – cat texture; *c* – tree texture [42]

The proposed algorithm facilitated solution of the texture segmentation task by providing a segmentation technique with helpful additional information about the analyzed image. The computer program was tested on natural grayscale images.

The other texture algorithm was developed on the base of calculation of histograms of brightness, contrast, and contour orientations. We calculated the brightness, contrast, and contour orientation histograms of the images and use them as features and inputs to the Random Subspace Classifier (RSC) neural classifier. Our recognition system is based on a special neural network, the RSC that is the version of RTC. The only difference of the RSC from the RTC is that not all input parameters are involved in the operation of the system. From the entire set of input parameters, a subset is selected for each block.

This study was to develop and test a recognition system for the Colorado potato beetles (example is presented in **Fig. 2.6**) on the plants [43]. This task is very important for localizing the beetles and reducing the pesticide volume used to protect the harvest. We employ a beetle image dataset representing different beetle positions and varying numbers of beetles. These images were collected from the Internet. We obtained the best recognition rate of 85 %.

a *b*

Fig. 2.6 Examples of Colorado beetle images: *a* – original images; *b* – marked images for RSC

This investigation was continuing for Mexican beetles' recognition [44].

The aim of this study is to develop a method for automated classification of blood cell images for the diagnosis of various diseases, which allows increasing the recognition rate in the diagnosis of diseases. To achieve the goal, the following tasks are required:

– development of algorithms of feature extraction from images;

– development of neural networks as element of decision making;

– programming of the algorithms of feature extraction from images and neural network method;

– testing them on selected image database.

The main hypothesis of the study is based on our experience in development of neural classifiers.

We developed different types of neural classifiers as RTC, Limited Receptive Area Classifier (LIRA), Permutation Coding Neural Classifier (PCNC).

Assumptions accepted in the work are the following:

– we can extract different features of the images of the blood as from patients with diseases and from images of healthy persons;

– neural network can be trained and after that can be used to recognize new images of blood cells.

2.3 Methodology

2.3.1 Texture recognition in blood smear images

The task of image recognition of lymphocytes affected by ALL consisted from several steps. The first step requires selecting the cells that are affected by the disease. A typical blood image consists of three components: red blood cells (erythrocytes), leukocytes, and platelets. Therefore, we will focus on leukocytes, specifically lymphocytes. **Fig. 2.7** depicts a sample image from the ALL-IDB2 database [27] containing four healthy cells from patients without ALL and four probable blast cells. The second step includes the calculation of texture features. The third step includes the training of neural classifier.

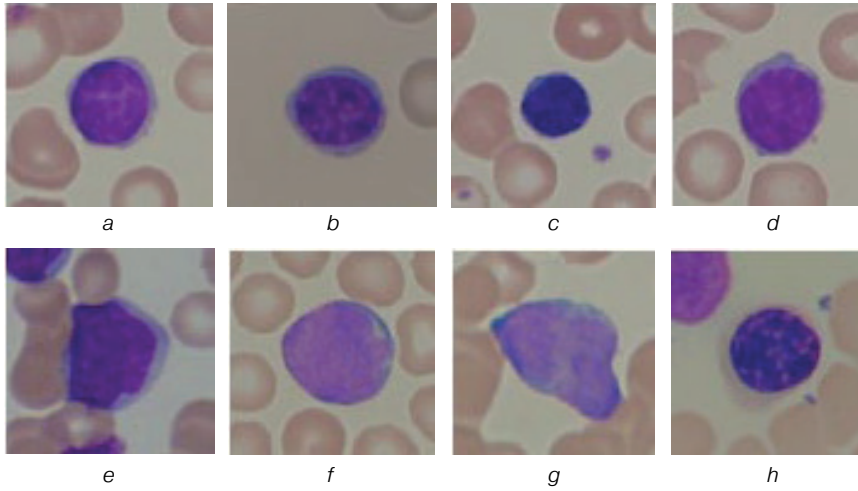

Fig. 2.7 Images from the ALL-IDB2 database: *a–d* present healthy cells from patients without ALL; *e–h* present probable lymphoblasts from patients with ALL [27]

The method of French-American-British co-operative group (FAB) is used in medicine for a long time to classify a cell as a blast or normal [45]. The FAB classification for acute lymphoblastic leukemia is divided into three categories:

L1: Lymphoblasts are small and homogeneous. The nuclei are round and regular with little cleavage and discrete nucleoli. The cytoplasm is scant and usually without vacuole.

L2: Lymphoblasts are massive and diverse. The nuclei are irregular and frequently cleft. Nucleoli are present. The cytoplasm may contain vacuoles, and its volume is variable but typically abundant.

L3: Lymphoblasts range in size from moderate to large and are homogeneous. One or more prominent nucleoli are present. The shape of the nuclei is regular and round-oval. The cytoplasm is moderate in volume and contains numerous prominent vacuoles.

Some characteristics of lymphocytes and lymphoblasts are as follows:

– a lymphoblast is approximately 10–18 μm in size, while a mature lymphocyte is about 17–20 μm;

– a lymphoblasts have a nuclear-to-cytoplasmic ratio of 4:1, while lymphocytes have a ratio of 2:1;

– a lymphoblasts contain 1–2 nucleoli, whereas mature lymphocytes lack nucleoli;

– in contrast to lymphoblasts, the chromatin of lymphocytes is dense and clustered;

– a lymphoblast cytoplasm is devoid of granules, whereas few azurophilic granules are present in lymphocytes;

– the stained lymphoblast cytoplasm turns medium blue with a dark blue border, whereas the stained lymphocyte cytoplasm turns light blue.

In terms of area, perimeter, texture, circularity, and nucleus-cytoplasm ratio, **Table 2.2** depicts the morphological characteristics of affected and normal cells for diagnosing ALL [9].

Therefore, the local characteristics of the blood images are extracted first in terms of texture. For this purpose, the following structure of the proposed texture recognition system is presented in **Fig. 2.8**.

Table 2.2 Morphological characteristics for ALL diagnostic [9]

Characteristic	L1	L2	L3	Normal	Mathematical relation
Cell size	Small	Large	Large	17–20 μm	Area and perimeter
Cell chromatin	Fine or grume	Fine	Fine	Dense and clumped	Texture from histograms
Nucleus shape	Regular, may have indentations	Irregular, may have indentations	Regular, oval or round	Regular without indentations	Area, circularity and nucleus-cytoplasm relation
Nucleolus	Does not distinguish	One or more, big prominent	One or more, big prominent	Without nucleolus	Texture from histograms
Cytoplasm	Scarce	Moderately abundant	Abundant	Normal	Area and nucleus-cytoplasm relation

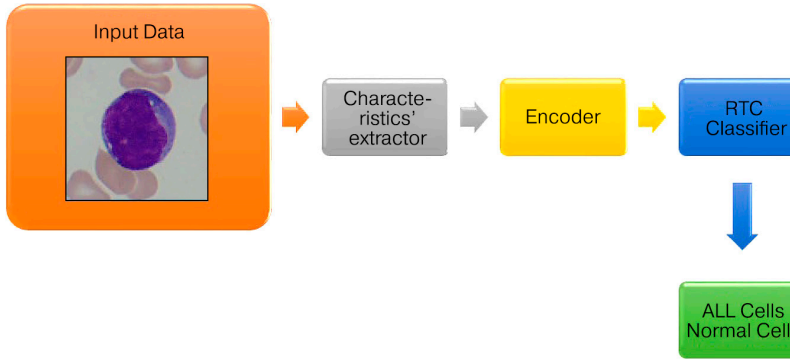

Fig. 2.8 RTC classifier's structure

The extracted characteristics are presented to the input of the encoder. The encoder generates the output binary vector, which is then presented to the input of the single-layer neural classifier, and, finally, the classifier's output provides the recognized class, which in this case consists of two classes, healthy cell, and affected cell [37, 38, 45]. In **Table 2.2** the morphological characteristics for ALL diagnostic are presented [9].

2.3.2 Characteristic extractor

This module is based on the image processing procedure. It will provide us with the necessary information to distinguish a leukocyte from the other cells in the peripheral blood image, as well as the characteristics that distinguish a lymphocyte from a lymphoblast. This system includes color, texture, and border characteristics represented through their histograms, and these characteristics are obtained from the nucleus of every lymphocyte or lymphoblast discovered by the system. To achieve this, an initial image is scanned by moving a (20×20)-pixel window with a 10-pixel step. Three brightness, contrast, and contour orientation histograms were calculated for each window. Each histogram consists of 16 components, for a total of 48 components or features that will comprise the input vector (X_1, …, X_n) for the RTC classifier.

2.3.3 Characteristic encoder

The characteristic encoder converts the extracted properties given by the property or characteristics extractor into a binary vector. Encoding then creates a binary

vector (b_1, ..., b_s) for each characteristic vector (X_1, ..., X_n). This vector is presented to the classifier's next layer. The proposed neural classifier has the Hebbian training rule as a one-layer perceptron.

2.3.4 Random Threshold Classifier (RTC)

It is proposed a neural classifier with high performance both in training and processing. Random Threshold Classifier (RTC) is the name of this classifier [46–48]. The basic idea is to create multilayer perceptrons with a single layer of training connections, which allows a rapid training rate. Placing additional non-modifiable layers of connections and binary neurons that allow nonlinear transformations of spatial input parameters to binary spatial parameters with extremely high dimensions improves image recognition accuracy.

The RTC structure is depicted in **Fig. 2.9**. The network structure is comprised by s similar blocks with a neural output in each (b_1, ..., b_s) block. A complete set of (X_1, ..., X_n) characteristics supplies each block's inputs.

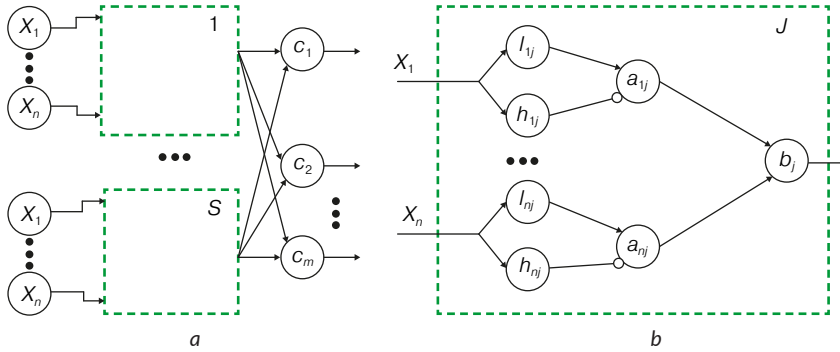

Fig. 2.9 RTC neural classifier: *a* – the whole structure; *b* – structure of one block

Each X_i characteristic feeds two neurons, h_{ij} and l_{ij}, where i ($i = 1, 2, ..., n$) represents the input features for neurons in every block j. The threshold value of l_{ij} falls below the threshold value of h_{ij}. A unique random procedure determines these values. The output of the l_{ij} neuron is connected to the excited input of the next a_{ij} neuron, and the output of the h_{ij} neuron is connected to the inhibited input of a a_{ij} neuron. At the output of a a_{ij} neuron, the signal only occurs when the signal X_i is between l_{ij} and h_{ij}.

All outputs of a neurons within a j block are connected to the excited inputs of a b_i neuron, which represents the whole neural block output.

The threshold value of the b_j neuron equals the number of a_{ij} neurons, i.e., in the b_j neural output, the signal is generated when all a_{ij} neurons within the block are excited. The neural output for each block is connected to all the neural inputs of the (c_i) classifier through trainable connections (w_{ij}), which are modified at each training stage. Each neuron in this layer represents a classification response of the system, and the neuron with the greatest excitation value is chosen. The classifier works in two ways: training and recognition. For training connections, Hebbian rule is applied:

$$w_{jc}(t+1) = w_{jc}(t)+a; \tag{2.5}$$

$$w_{ji}(t+1) = w_{ji}(t)-a, \tag{2.6}$$

in which the c index represents the correct class, and the index i represents the incorrect class.

The neural network undergoes a training phase whose objective is to correctly recognize as many patterns as possible. The training consists of decreasing all the weights of the connections of the incorrect class and increasing those of the correct class, which leads us to supervised or master training.

In order to understand the principles mentioned above, we will interpret them geometrically, as shown in **Fig. 2.10**, for a case with three input features X_1, X_2, and X_3, so for three-dimension task instead of n dimension as presented in **Fig. 2.9, *a***.

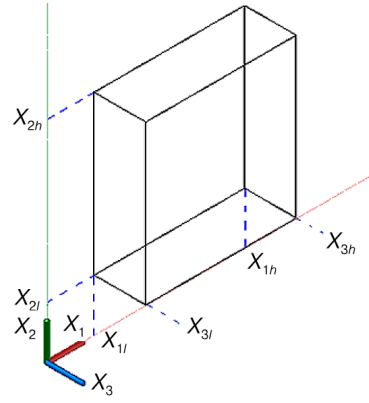

Fig. 2.10 Geometric identification of the neuron

When the point representing the feature vector is inside the represented rectangle, the output neuron that is corresponded to the block output will be stimulated or active. Since the classifier contains a sufficient number of blocks with similar (neurons with thresholds) but different characteristics (different values of thresholds), all spatial features appear in a sufficient number of multidimensional parallelepipeds located on random planes and having random sizes. We demonstrate the geometrical interpretation only for three input parameters.

The number of parallelepipeds is equal to the number of blocks (b_1, ..., b_s). We can analyze the point in space $\left(X_1^*,\ X_2^*,\ X_3^*\right)$ shown in **Fig. 2.11** where numerous (V) parallelepipeds have been covered. With the training process and definition of weights between penultimate and last layers (w_{ij}) the neural classifier can divide the parametric space on different classes.

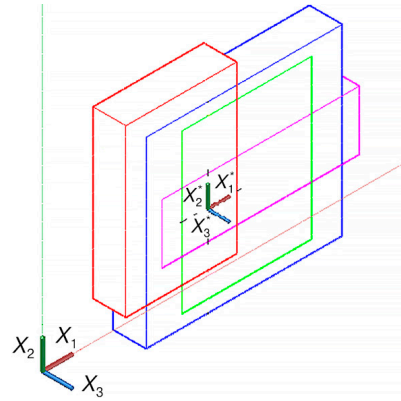

Fig. 2.11 A geometric representation of the classifier

V is the random value for different points in space, and typically classifier parameters are chosen to obtain an average value V.

Taking into account the need to distinguish three classes, let the point $\left(X_1^*,\ X_2^*,\ X_3^*\right)$ belong to the second class. If the point is far from the class boundary, it is covered by parallelepipeds whose volumes lie within the class boundary of the second class. This implies that during the training process, the weights of the connections between neurons belonging to b_i and the neural outputs of the second class will be greater than the weights of the connections of b_i neurons with first-class neurons. Therefore, the point $\left(X_1^*,\ X_2^*,\ X_3^*\right)$ will be recognized as belonging to the second class.

2.3.5 Database description: ALL-IDB

ALL-IDB [27] is a public imaging database of peripheral blood samples from healthy individuals and leukemia patients. These samples were gathered by professionals at the M. Tettamanti Research Center for Childhood Leukemia and Hematological Diseases in Monza, Italy. The ALL-IDB database is comprised of two different versions, ALL-IDB1 and ALL-IDB2, and its images are in JPG format with 24-bit color depth. ALL-IDB1 is comprised of 108 original RGB images captured with a laboratory optical microscope and an Olympus Optical C2500L camera or a Canon Power Shot G5 camera. The resolution of the first 33 images is 1712×1368, while the remaining images have a resolution of 2592×1944.

The images were taken at different microscope magnifications, ranging from 300 to 500, which brought the differences in color and brightness. ALL-IDB1 provides complete images containing cells and agglomerates; thus, it can be used to evaluate the segmentation capabilities of algorithms, as well as the image preprocessing techniques or the classification systems. ALL-IDB2 is a collection of clipped areas of interest from blastic and healthy cells extracted from ALL-IDB1. It consists of 260 images, with 50 % of these depicting lymphoblasts.

2.4 Results, experiments and discussion

To present the results obtained by the RTC neural classifier, the aforementioned ALL-IDB2 database was employed, along with 100 images, of which 60 were used for training and the remaining 40 for testing. To calculate the recognition error percentage, the total number of windows is first obtained using the following equation:

$$NTV = \left(\frac{W}{\frac{w}{2}} - 1\right) \times \left(\frac{H}{\frac{h}{2}} - 1\right) \times NIB, \tag{2.7}$$

where NTV is a total number of windows; W is an image width; H is an image height; w is a window width; h is a window height; NIB is a number of images stored in the database.

The percentage error is computed by the following equation:

$$x = \frac{100 \times N_{error}}{NTV}\,\%, \tag{2.8}$$

where N_{error} is the number of windows that the system did not recognize correctly in the recognition stage.

Before presenting the results of calculations, we want to describe in detail the algorithms of the system.

The graphical user interface is comprised of a menu with the following options (**Fig. 2.12**): Mask generation, Open Image-Coding, Training, and Recognition.

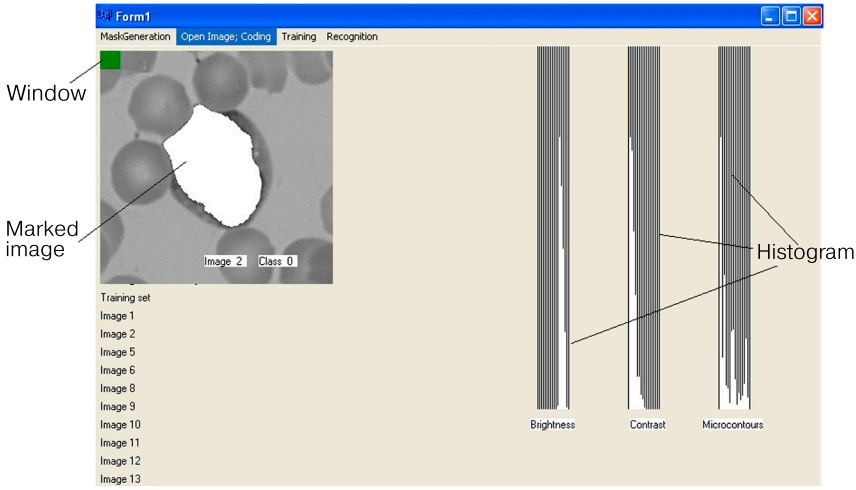

Fig. 2.12 Program system

In the first option, "Mask generation" is the first part of the RTC classifier structure. In this stage all *S* blocks were generated with neurons with random thresholds (**Fig. 2.9, *b***) and they were saved and used in work process. In the case that we analyze in this work $S = 64000$ (**Fig. 2.9, *a***). In the first menu item (in the process of system preparation) the program randomly selects images from the ALL-IDB database for the training and test phases, where half of the images are selected for training and the other half for testing.

The following option – "Open Image-Coding" – is where the 100 images in the database are opened and encoded. It is performed a scan of the whole image with a (20×20 pixels) window (in **Fig. 2.12** the window is presented with green colour). The step of scanning corresponds to the half of the window size. Every window is a sample for the neural network. For every window we calculate three histograms that are presented in **Fig. 2.12**. These are the histogram of brightness, histogram of contrast

and histogram of micro contours orientations. So, we have three groups of features. Every group has 16 features. So, in total we have 48 input features for every block. In our case, $n=48$ (**Fig. 2.9, *a***).

In our task there are three classes, $m=3$ (**Fig. 2.9, *a***). One of them corresponds to class zero (0), which helps us identify the background of the image; the next class (1) for the case where there are no cells affected by the ALL disease, i.e., healthy cells, and finally, class two (2) where there are cells affected by the ALL disease (lymphoblasts). For each window (input sample) the histograms of brightness, contrast, and micro-contour orientation are computed, after the work of blocks (**Fig. 2.9, *a***) the system has a neural output in each (b_1, ..., b_s) block. The vector (b_1, ..., b_s) is a binary vector that is a code of window for the network structure.

Once this process is finished, the "Training" option will begin, which, as mentioned above, consists of decreasing all the connections weights of the incorrect class and increasing those of the correct class. The objective of the training is to correctly recognize the most significant number of patterns. The training process is a supervised training (training with a teacher). For this reason, we marked all images that participate in our experiments for the process of training (**Fig. 2.12**). The system has information about which class the considered window belongs to. If the window falls on the image area where two or three classes have their representation, then choose the class that has the largest number of pixels.

Finally, there is the "Recognition" option in which the remaining half of the images, which were not used in the training phase, is used. At this stage, we can obtain the number of errors, and with these, we can calculate the percentage of recognition rate of our system.

It is worth mentioning that we obtain 48 texture characteristics. In **Fig. 2.13** one example of the results of RTC work are demonstrated. The image is green because it was scanned with window of green colour.

We investigated the influence of the window size to the recognition rate. To obtain statistically stable and confident results we did with every window size five experiments and calculated the average error number. The results are presented in **Table 2.3**.

Five experiments for each window size help us to decrease the influence of the randomly selected parameter values.

The best results were obtained for window sizes\ (20×20) and (40×40) pixels. Trend of this investigation demonstrates that with large window we can obtain the better results.

Table 2.4 shows a comparison of the different methods employed by various authors, as well as the results obtained using our proposed RTC method.

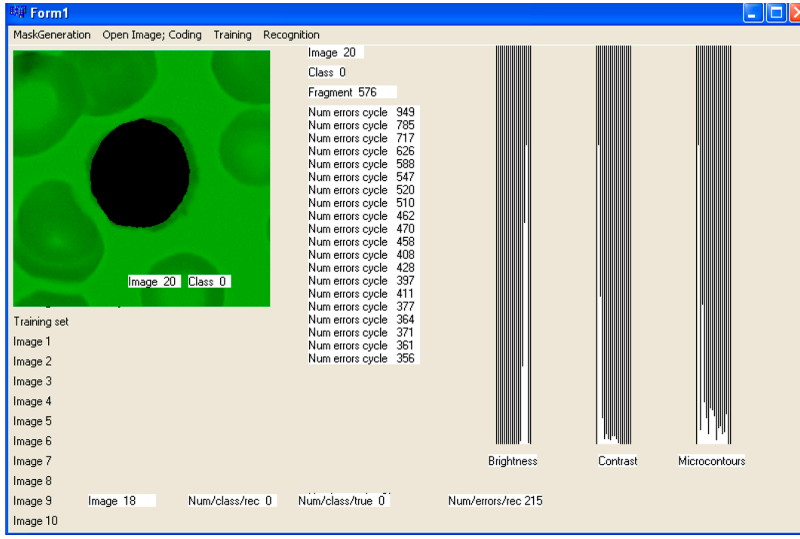

Fig. 2.13 Development environment

Table 2.3 Experiments with different window size

Window size	10×10		20×20		30×30		40×40	
	Errors	Recog-nition Rate (%)	Errors	Recog-nition Rate (%)	Errors	Recog-nition Rate (%)	Errors	Recog-nition Rate (%)
				Run				
1	7048	86.13	215	98.24	347	93.33	88	96.87
2	7040	86.14	205	98.32	371	92.87	79	97.19
3	6090	88.01	235	98.07	261	94.98	108	96.15
4	7030	86.16	195	98.4	325	93.75	90	96.79
5	7050	86.12	183	98.5	355	93.18	110	96.08
Average		**86.512**		**98.306**		**93.622**		**96.616**

Experiments with RTC demonstrate that the results were superior to the best result obtained in [37] and significantly superior to those obtained using SVM-G in [38]. It should be noted that all mentioned methods utilize the ALL-IDB database. A detailed description of these methods is beyond the scope of this paper; instead, we will compare our outcomes to theirs.

Table 2.4 The average recognition rate for the ALL-IDB database (%)

Authors	Gayathri & Jyothi [49]	Putzu, Caocci, Di Ruberto [10]	Di Ruberto, Loddo, Puglisis [24]	Shakhawan Hares Wady [37]	Alagu & Bagan [38]	Curtidor, Kussul, Baydyk, Mammadova [50]
Methods	CNN	IPT	Deep Learning	LDNP+M-WDT	SVM-G	RTC
Recognition (%)	93	93.2	94.1	97.69	95.3	98.3

As shortcomings of this study we can noted that we used only one image database. For effective application of neural classifiers, it is very important to increase the number of images for training process. The time of training may demand hours or days. But it is possible to use pre-trained neural networks.

In the future we can use other image databases for diagnostic not only ALL but other diseases where image analysis is important for doctors and they need assistance by computer systems.

It will be interested to add to texture characteristics the other features, for example, the form parameter that can be calculated as perimeter of the cell divided to the area of the cell.

To our opinion the difficulties that we may encounter in future are connected with quality of images. Image set quality may include, for example, excessively noisy images, mislabeled duplicate images, uneven image resolution, varying class sample sizes that can demand special preliminary preparation of image dataset.

2.5 Conclusions

The neural classifier with the title the Random Threshold Classifier (RTC) was used to recognize the texture of human blood cells images, with a focus on white blood cells (leukocytes). The classification of healthy lymphocytes and diseased lymphocytes, also known as lymphoblasts was selected as test task. At the input of the RTC classifier, brightness histograms, contrast histograms, and micro-contour orientation histograms were calculated for each image from the ALL-IDB database, generating a characteristics vector that would be the input of the neural classifier. We developed the specialized program using C++ to extract the characteristics of interest and to train and test the images with RTC neural classifier. The program system permits us to recognize where the healthy or diseased cells are detected.

The RTC neural classifier demonstrated a higher recognition percentage of 98.3 % compared with 95.3 % of the SVM-G and of 97.69 %. So, our neural classifier may be used to identify the lymphoblasts using images of the healthy or diseased cells.

Conflict of interest

The authors declare that they have no conflict of interest in relation to this research, whether financial, personal, authorship or otherwise, that could affect the research and its results presented in this paper.

Acknowledgment

The authors would like to thank Labati et al for sharing the Acute Lymphoblastic Leukemia image database (ALL-IDB).

We thank the Regional Center of Investigations Dr. Hideyo Noguchi, from the Autonomous University of Yucatán, for the tissue image database.

The special acknowledgment from Dra. Airam Curtidor for poststudent grant del CONAHCYT, Mexico.

References

1. González, C. (2011). Recognition of Textures in Medical Images. UNAM. Available at: https://xdoc.mx/documents/tesis-unam-5ddae474b690d
2. Mammadova, M., Bayramov, N., Jabrayilova, Z. (2021). Development of the principles of fuzzy rule-based system for hepatocelular carcinoma staging. EUREKA: Physics and Engineering, 3, 3–13. doi: https://doi.org/10.21303/2461-4262.2021.001829
3. Mammadova, M., Jabrayilova, Z. (2022). Synthesis of decision making in a distributed intelligent personnel health management system on offshore oil platform. EUREKA: Physics and Engineering, 4, 179–192. doi: https://doi.org/10.21303/2461-4262.2022.002520
4. Huerta Aragonés, J., Cela de Julián, E. E. (2019). Practical Hematology: Interpretation of the Complete Blood Count and Coagulation Tests. Pediatric Update Congress 2019. Madrid: Lúa Ed. 3.0, 507–528.

5. Rahi, M. S., Jindal, V., Reyes, S.-P., Gunasekaran, K., Gupta, R., Jaiyesimi, I. (2021). Hematologic disorders associated with COVID-19: a review. Annals of Hematology, 100 (2), 309–320. doi: https://doi.org/10.1007/s00277-020-04366-y
6. Zini, G., Bellesi, S., Ramundo, F., d'Onofrio, G. (2020). Morphological anomalies of circulating blood cells in COVID-19. American Journal of Hematology, 95 (7), 870–872. doi: https://doi.org/10.1002/ajh.25824
7. Salib, C., Khattar, P., Cheng, J., Teruya-Feldstein, J. (2020). Atypical Peripheral Blood Cell Morphology in COVID-19 (Sars-CoV-2) Patients from Mount Sinai Health System in New York City. Blood, 136, 26–27. doi: https://doi.org/10.1182/blood-2020-142581
8. Introcaso, G., Biondi, M. L. (2022). Morphological anomalies of blood cells in COVID-19 patients. Open Journal of Clinical and Medical Images, 2 (2), 1080. doi: https://doi.org/10.52768/2833-2725/1080
9. Guía de Referencia Rápida (2018). Diagnosis and Treatment Lymphoblastic Leukemia Acute In The Adult. Instituto Mexicano del Seguro Social. Dirección de Prestaciones Médicas. Unidad de Atención Médica. Coordinación de Unidades Médicas de Alta Especialidad. División de Excelencia Clínica.
10. Putzu, L., Caocci, G., Di Ruberto, C. (2014). Leucocyte classification for leukaemia detection using image processing techniques. Artificial Intelligence in Medicine, 62 (3), 179–191. doi: https://doi.org/10.1016/j.artmed.2014.09.002
11. Piuri, V., Scotti, F. (2004). Morphological classification of blood leucocytes by microscope images. 2004 IEEE International Conference OnComputational Intelligence for Measurement Systems and Applications, 2004. CIMSA. doi: https://doi.org/10.1109/cimsa.2004.1397242
12. Ruberto, C. D., Putzu, L. (2014). Accurate Blood Cells Segmentation through Intuitionistic Fuzzy Set Threshold. 2014 Tenth International Conference on Signal-Image Technology and Internet-Based Systems. doi: https://doi.org/10.1109/sitis.2014.43
13. Ongun, G., Halici, U., Leblebicioglu, K., Atalay, V., Beksac, M., Beksac, S. (2001). An automated differential blood count system. 2001 Conference Proceedings of the 23rd Annual International Conference of the IEEE Engineering in Medicine and Biology Society. doi: https://doi.org/10.1109/iembs.2001.1017309
14. Mohamed, M., Far, B., Guaily, A. (2012). An efficient technique for white blood cells nuclei automatic segmentation. 2012 IEEE International Conference on Systems, Man, and Cybernetics (SMC). doi: https://doi.org/10.1109/icsmc.2012.6377703
15. Mohammed, E. A., Mohamed, M. M. A., Far, B. H., Naugler, C. (2014). Peripheral blood smear image analysis: A comprehensive review. Journal of Pathology Informatics, 5 (1), 9. doi: https://doi.org/10.4103/2153-3539.129442

16. Madhloom, H. T., Kareem, S. A., Ariffin, H., Zaidan, A. A., Alanazi, H. O., Zaidan, B. B. (2010). An Automated White Blood Cell Nucleus Localization and Segmentation using Image Arithmetic and Automatic Threshold. Journal of Applied Sciences, 10 (11), 959–966. doi: https://doi.org/10.3923/jas.2010.959.966
17. Halim, N. H. A., Mashor, M. Y., Hassan, R. (2011). Automatic Blasts Counting for Acute Leukemia Based on Blood Samples. International Journal of Research and Reviews in Computer Science, 2 (4), 971–976. Available at: https://www.proquest.com/scholarly-journals/automatic-blasts-counting-acute-leukemia-based-on/docview/903775031/se-2
18. Tang, J. (2010). A color image segmentation algorithm based on region growing. 2010 2nd International Conference on Computer Engineering and Technology. doi: https://doi.org/10.1109/iccet.2010.5486012
19. Navon, E., Miller, O., Averbuch, A. (2005). Color image segmentation based on adaptive local thresholds. Image and Vision Computing, 23 (1), 69–85. doi: https://doi.org/10.1016/j.imavis.2004.05.011
20. Mahameed, A. I., Ahmed, M. K., Abdullah, N. B. (2022). Iris recognition method based on segmentation. EUREKA: Physics and Engineering, 2, 166–176. doi: https://doi.org/10.21303/2461-4262.2022.002341
21. Kumar, R. S., Verma, A., Singh, J. (2007). Color Image Segmentation and Multi-Level Thresholding by Maximization of Conditional Entropy. International Journal of Computer and Information Engineering, 1 (6), 1633–1641. doi: https://doi.org/10.5281/zenodo.1059435
22. Scotti, F. (2005). Automatic morphological analysis for acute leukemia identification in peripheral blood microscope images. CIMSA. 2005 IEEE International Conference on Computational Intelligence for Measurement Systems and Applications, 2005. doi: https://doi.org/10.1109/cimsa.2005.1522835
23. Mahmood, N. H., Lim, P. C., Mazalan, S. M., Razak, M. A. A. (2013). Blood cells extraction using color based segmentation technique. Int. J. Life Sci. Biotechnol. Pharma Res, 2 (2), 233–240. Available at: https://www.researchgate.net/publication/289676562_Blood_cells_extraction_using_color_based_segmentation_technique
24. Di Ruberto, C., Loddo, A., Puglisi, G. (2020). Blob Detection and Deep Learning for Leukemic Blood Image Analysis. Applied Sciences, 10 (3), 1176. doi: https://doi.org/10.3390/app10031176
25. Skuratov, V., Kuzmin, K., Nelin, I., Sedankin, M. (2020). Application of a convolutional neural network and a Kohonen network for accelerated detection and recognition of objects in images. EUREKA: Physics and Engineering, 4, 11–18. doi: https://doi.org/10.21303/2461-4262.2020.001360

26. Skuratov, V., Kuzmin, K., Nelin, I., Sedankin, M. (2020). Application of kohonen self-organizing map to search for region of interest in the detection of objects. EUREKA: Physics and Engineering, 1, 62–69. doi: https://doi.org/10.21303/2461-4262.2020.001133
27. Labati, R. D., Piuri, V., Scotti, F. (2011). All-IDB: The acute lymphoblastic leukemia image database for image processing. 2011 18th IEEE International Conference on Image Processing. doi: https://doi.org/10.1109/icip.2011.6115881
28. Acharya, V., Kumar, P. (2019). Detection of acute lymphoblastic leukemia using image segmentation and data mining algorithms. Medical & Biological Engineering & Computing, 57 (8), 1783–1811. doi: https://doi.org/10.1007/s11517-019-01984-1
29. Mirmohammadi, P., Ameri, M., Shalbaf, A. (2021). Recognition of acute lymphoblastic leukemia and lymphocytes cell subtypes in microscopic images using random forest classifier. Physical and Engineering Sciences in Medicine, 44 (2), 433–441. doi: https://doi.org/10.1007/s13246-021-00993-5
30. He, K., Zhang, X., Ren, S., Sun, J. (2016). Identity Mappings in Deep Residual Networks. Computer Vision – ECCV 2016, 630–645. doi: https://doi.org/10.1007/978-3-319-46493-0_38
31. Rodrigues, L. F., Backes, A. R., Travençolo, B. A. N., de Oliveira, G. M. B. (2022). Optimizing a Deep Residual Neural Network with Genetic Algorithm for Acute Lymphoblastic Leukemia Classification. Journal of Digital Imaging, 35 (3), 623–637. doi: https://doi.org/10.1007/s10278-022-00600-3
32. Chand, S., Vishwakarma, V. P. (2022). A novel Deep Learning Framework (DLF) for classification of Acute Lymphoblastic Leukemia. Multimedia Tools and Applications, 81 (26), 37243–37262. doi: https://doi.org/10.1007/s11042-022-13543-2
33. Rejula, M. A., Amutha, S., Shilpa, G. M. (2023). Classification of acute lymphoblastic leukemia using improved ANFIS. Multimedia Tools and Applications, 82 (23), 35475–35491. doi: https://doi.org/10.1007/s11042-023-15113-6
34. Renuka, T. V., Surekha, B. (2021). Acute-Lymphoblastic Leukemia Detection Through Deep Transfer Learning Approach of Neural Network. Lecture Notes in Networks and Systems, 163–170. doi: https://doi.org/10.1007/978-981-33-4073-2_17
35. Litjens, G., Kooi, T., Bejnordi, B. E., Setio, A. A. A., Ciompi, F., Ghafoorian, M. et al. (2017). A survey on deep learning in medical image analysis. Medical Image Analysis, 42, 60–88. doi: https://doi.org/10.1016/j.media.2017.07.005
36. Alam, A., Anwar, S. (2021). Detecting Acute Lymphoblastic Leukemia Through Microscopic Blood Images Using CNN. Trends in Wireless Communication and Information Security, 207–214. doi: https://doi.org/10.1007/978-981-33-6393-9_22

37. Wady, S. H. (2022). Classification of Acute Lymphoblastic Leukemia through the Fusion of Local Descriptors. UHD Journal of Science and Technology, 6 (1), 21–33. doi: https://doi.org/10.21928/uhdjst.v6n1y2022.pp21-33
38. Alagu, S., Bagan, K. B. (2019). Acute Lymphoblastic Leukemia Diagnosis in Microscopic Blood Smear Images Using Texture Features and SVM Classifier. Alliance International Conference on Artificial Intelligence and Machine Learning (AICAAM), 175–186. Available at: https://www.researchgate.net/publication/343444613_Acute_Lymphoblastic_leukemia_diagnosis_in_microscopic_blood_smear_images_using_texture_features_and_SVM_classifier
39. González, C., Baydyk, T., Kussul, E. (2010). Recognition of Textures in Medical Images. 1st International Congress on Instrumentation and Applied Sciences ICIAS.
40. Schwartz, R. (1984). Pat. No. US4433912A. Method and a circuit for determining a contour in an image. published: 28.02.1984. Available at: https://patents.google.com/patent/US4433912A/en?oq=4433912+US
41. Duda, R., Hart, P., Stork, D. (2000). Pattern classification. John Wiley & Sons, Inc., 680.
42. Goltsev, A., Gritsenko, V., Kussul, E., Baidyk, T. (2015). Finding the Texture Features Characterizing the Most Homogeneous Texture Segment in the Image. Lecture Notes in Computer Science, 287–300. doi: https://doi.org/10.1007/978-3-319-19258-1_25
43. Roldan-Serrato, L., Baydyk, T., Kussul, E., Escalante-Estrada, A., Rodriguez, M. T. G. (2015). Recognition of pests on crops with a random subspace classifier. 2015 4th International Work Conference on Bioinspired Intelligence (IWOBI). doi: https://doi.org/10.1109/iwobi.2015.7160138
44. Roldán-Serrato, K. L., Escalante-Estrada, J. A. S., Rodríguez-González, M. T. (2018). Automatic pest detection on bean and potato crops by applying neural classifiers. Engineering in Agriculture, Environment and Food, 11 (4), 245–255. doi: https://doi.org/10.1016/j.eaef.2018.08.003
45. Bennett, J. M., Catovsky, D., Daniel, M., Flandrin, G., Galton, D. A. G., Gralnick, H. R., Sultan, C. (1976). Proposals for the Classification of the Acute Leukaemias French-American-British (FAB) Co-operative Group. British Journal of Haematology, 33 (4), 451–458. doi: https://doi.org/10.1111/j.1365-2141.1976.tb03563.x
46. Baidyk, T., Kussul, E., Makeyev, O. (2005). Texture Recognition with Random Subspace Neural Classifier. WSEAS Transactions on Circuits and Systems, 4 (4), 319–324.
47. Baidyk, T., Kussul, E., Makeyev, O. (2008). General purpose image recognition systems based on neural classifiers. Progress in Neurocomputing Research. Chap. 3. NOVA Publishers, 83–114.

48. Kussul, E., Makeyev, O., Baidyk, T., Martín-Gonzalez, A., Toledo-Ramirez, G. (2011). Some Applications of Computer Vision Systems in Micromechanics. Computer Vision. Nova Science Publishers.
49. Gayathri, S., Jyothi, R. L. (2018). An Automated Leucocyte Classification for Leukemia Detection. International Research Journal of Engineering and Technology (IRJET), 5 (5), 4254–4264. Available at: https://www.irjet.net/archives/V5/i5/IRJET-V5I5908.pdf
50. Curtidor, A., Kussul, E., Baydyk, T., Mammadova, M. (2023). Analysis and automated classification of images of blood cells to diagnose acute lymphoblastic leukemia. EUREKA: Physics and Engineering, 5, 177–190. doi: https://doi.org/10.21303/2461-4262.2023.003070